Chapter 1

DETECTION OF MULTIPLY SCATTERED LIGHT IN OPTICAL COHERENCE MICROSCOPY

K. K. Bizheva, A. M. Siegel
Dept. of Physics and Astronomy
Tufts University, Massachusetts, USA

A. K. Dunn and D. A. Boas
Nuclear Magnetic Resonance Center
Massachusetts General Hospital, Harvard Medical School
13th St., Bldg. 149, Charlestown, Massachusetts 02129, USA
dboas@nmr.mgh.harvard.edu

Abstract In this study a number of experimental and computational methods were employed to examine the effect of multiply scattered light detection on image quality and penetration depth of optical coherence microscopy (OCM) in turbid media. Measurements of the OCM resolution at different optical depths in the scattering media reveal that detection of multiply scattered light causes significant degradation of the lateral and axial resolution and that the deterioration effect is dependent on the turbid media scattering anisotropy and the numerical aperture (NA) of the imaging objective.

Keywords: scattering, optical coherence microscopy, imaging, diffusion

Introduction

A major problem in biomedical optical imaging is the fact that image quality degrades with depth penetration: the deeper the imaged object is buried in turbid media like tissue, the less precise is the determination of it's location, size, shape and optical properties. Various microscopy techniques like confocal (CM) and optical coherence microscopy / tomography (OCM/OCT) [4-6] can produce high- resolution images (1-10 μm) in tissue by selectively detecting mainly ballistic and single scattered light. The image penetration depth though, is

P. Sebbah (ed.), Waves and Imaging through Complex Media, 277–298.

typically limited to a range of a few hundred microns up to a millimeter. Other methods like diffuse optical tomography (DOT) [7, 8] utilize the statistical properties of light thus permitting imaging of objects buried at a depth of a few centimeters at the expense of significantly reduced image quality (5-10 mm resolution).

Currently, the intermediate regime spanning between optical microscopy and DOT, where light is multiply scattered (a few photon scattering events) but not yet diffuse, is still relatively unexplored. Multiply scattered light reflected off an object embedded in a turbid medium carries a significant amount of information about the object location and properties. Therefore, development of new imaging modalities utilizing multiply scattered light will depend on how accurately this information can be interpreted. Proper interpretation though, will require thorough knowledge of the process of light interaction with the imaged object, and the turbid background for the imaging system employed. The detection of multiply scattered light and its deteriorating effect on image contrast, resolution and depth penetration has been partially investigated for both CM and OCM/OCT [9-13]. All of these studies employed measurements of back-scattered light in homogeneous or inhomogeneous samples as a function of the imaging lens focal depth or the total photon path length in the medium. A typical intensity profile acquired with an OCM system in a homogeneous scattering medium is shown in Fig. 1. For shallow depths of the focal point, the detected light is mainly single scattered resulting in an exponential decay (Beer-Lambert law) of the measured intensity (linear on a semi-log scale). As the objective focal point is translated deeper into the turbid medium, the contribution of multiply scattered light to the total intensity becomes more pronounced and after a certain depth the only light collected is diffuse . Since the transition from single scattered to diffuse light in the intensity profile (Fig. 1) is smooth, it is difficult to distinguish clearly the boundaries between regions where single scattered, multiply scattered and diffuse light are the dominant components of the measured intensity. The intensity profile in Fig. 1 poses various questions: when does detection of light that has scattered a few times become significant; when does the detected light become completely diffuse; how does partial detection of multiply scattered and diffuse light affect image contrast and resolution; how does the cumulative detection of multiply scattered light depend on the media optical properties, the instrument imaging geometry and the applied photon gating methods; is OCM imaging signal-to-noise or signal-to-background limited and can we define penetration depth limits as functions of the imaging geometry parameters and sample optical properties?

The main goal of this chapter is to provide answers to some of these questions. To do that a number of experimental and computational methods were utilized. To aid the investigation of the transition from single scattered to diffuse light detection in imaging systems, a new method, Dynamic Low Coherence

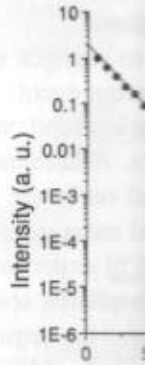

Figure 1. OCM intensity as a f
suspension. The straight line thro
single scattered light.

Interferometry (DLCI) was d
was derived from the Quasi-E
fuse Wave Spectroscopy (DW
pathlength selectivity of an
changes in the photon total
total pathlength in homogene
sensitive to the number of p
measurement. DLCI is limit
fore additional experimental
study the effect of multiply sc
point-spread function (PSF) .

The information presented
tion 1 reviews the methods u
scattered light and the subse
scribes in detail the experim
discussed in section 3. Last
study and presents an outline

1. METHODS FO
TRANSITION F
LIGHT DIFFUS

The following section revi
tion measurements) and comp

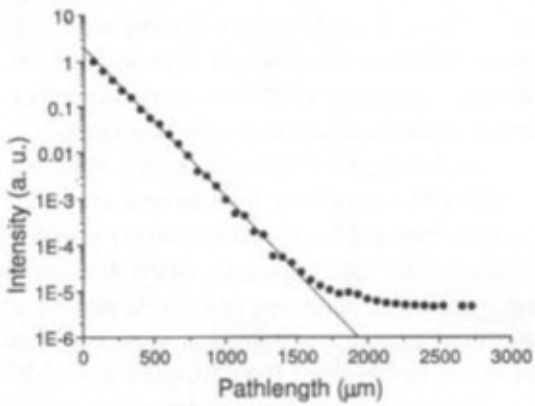

Figure 1. OCM intensity as a function of photon pathlength in a homogeneous scattering suspension. The straight line through the data points represents the expected attenuation of single scattered light.

Interferometry (DLCI) was developed in our lab [14, 15]. The idea for DLCI was derived from the Quasi-Elastic Light Scattering (QELS) [16, 17] and Diffuse Wave Spectroscopy (DWS) [18, 19, 20, 21, 22] theories and utilizes the pathlength selectivity of an OCT/OCM system. DLCI measures cumulative changes in the photon total momentum transfer as a function of the photon total pathlength in homogeneous, dynamic random media therefore it is more sensitive to the number of photon scattering events than a regular intensity measurement. DLCI is limited to measurements in dynamic systems, therefore additional experimental and computational techniques were employed to study the effect of multiply scattered light detection on the quality of the OCM point-spread function (PSF) .

The information presented in this book chapter is organized as follows: section 1 reviews the methods used to study the cumulative detection of multiply scattered light and the subsequent image degradation in OCM. Section 2 describes in detail the experimental and computational results, which are later discussed in section 3. Last section summarizes the accomplishments of this study and presents an outline of the future work.

1. METHODS FOR INVESTIGATING OF THE TRANSITION FROM SINGLE SCATTERING TO LIGHT DIFFUSION

The following section reviews the experimental (DLCI and OCM resolution measurements) and computational (Monte Carlo models) methods used to

investigate the transition from single scattered to diffuse light for the case of imaging in turbid media with OCM and OCT systems.

As a measurement method DLCI is sensitive to changes in the photon total momentum transfer, occuring after each scattering event. Therefore it can provide valuable insight on the effect of a turbid background on the OCM point-spread function in the absence of an imaged object. Additional information on the deteriorating effect of a scattering background on image quality (contrast and resolution) can be obtained from experimental measurements of the OCM lateral and axial resolution. Unfortunately, often in experimental studies detailed information on changes occurring at a single photon scale, necessary for understanding and modeling of the transition scattering regime, is lost. This type of information can be obtained from Monte Carlo (MC) models that can "label" photons, store information about the photon position, polarization state and momentum transfer after each scattering event and gate photons spatially (CM) and by their total path length (OCM).

1.1. DYNAMIC LOW COHERENCE INTERFEROMETRY

The principle of operation of DLCI is the same as of any standard interferometer with the only exception that one of the mirrors is substituted with the examined sample (Fig. 2). In our case the single-mode fiber optic interferometer is illuminated with light from an 850 nm super-luminescent diode (25 nm spectral bandwidth, 1.2 mW output power). The optical properties of the sample generate a distribution of optical path lengths in the sample arm, while the path length in the reference arm is determined solely by the position of the retroreflector. Interference is observed only when the optical path length difference between the reference and the sample arms is within the coherence length of the source. Thus, a "coherence gate" is used to select specific path lengths within the sample. The amplitude of the interference signal is therefore proportional to the path length dependent reflection/scattering properties of the sample. The position of the reference mirror (retroreflector) is adjusted in such a way as to align the coherence gate with the beam waist, thus optimizing the rejection of out-of-focus background light. The instrument lateral and axial resolution in air is determined by the objective NA and the size and shape of the spatial filter applied to result in confocal detection. In our case spatial filtering was realized by using a single mode fiber system. The instrument axial resolution is further enhanced for small NA objectives by the presence of a coherence gate.

For a fixed position of the reference mirror the photocurrent at the detector can we written as:

$$i_d \propto I_r + I_s + I^{fluct}(z,t)\,, \qquad (1)$$

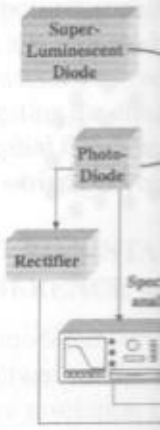

Figure 2. Experiment

where I_r (I_s) is the intensity
the cross term (or optical he
of the reference electric fie
$E_s(z)$ of the scattered light.
from changes in the amplitu
mirror is held fixed, the amp
Any dynamics in the turbid
a distribution of Doppler fre
medium, which causes phas
cross term intensity I^{fluct}(
the photo detector current i_d
particles undergoing Brown

where A is the amplitude of t
This equation does not acc
optically dilute suspension
therefore the scattering ang
of single scattered light, ass
cles, the power spectrum lin
coefficient D_B:

$\Omega =$

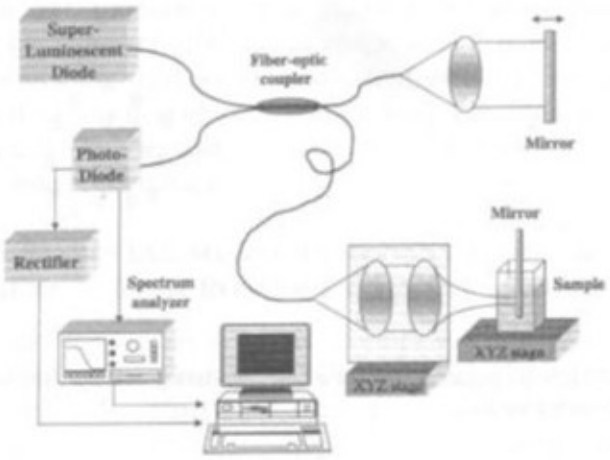

Figure 2. Experimental setup used for the DLCI and OCM measurements.

where I_r (I_s) is the intensity from the reference (sample) arm and $I^{fluct}(z,t)$ is the cross term (or optical heterodyne term) resulting from the coherent mixing of the reference electric field E_r with the path length dependent electric field $E_s(z)$ of the scattered light. Temporal fluctuations in the cross term may result from changes in the amplitude and/or phase of E_r or E_s. When the reference mirror is held fixed, the amplitude and the phase of E_r do not change over time. Any dynamics in the turbid sample such as flow or Brownian motion, result in a distribution of Doppler frequency shifts in the light propagating through the medium, which causes phase variations in $E_s(z)$, resulting in fluctuations in the cross term intensity $I^{fluct}(z,t)$. The power spectrum (a Fourier transform of the photo detector current i_d) derived for a system consisting of light scattering particles undergoing Brownian motion is a Lorentzian [16, 17]:

$$P(\omega) = \frac{1}{\Omega} \frac{A}{1 + \left(\frac{\omega}{\Omega}\right)^2}, \tag{2}$$

where A is the amplitude of the power spectrum and Ω is the spectrum linewidth. This equation does not account for the Ω=0 contribution of I_r and I_s. In an optically dilute suspension (Fig. 3a), light scatters only once before detection, therefore the scattering angle and polarization are well defined. For the case of single scattered light, assuming weak scattering and non-interacting particles, the power spectrum linewidth is proportional to the particle self-diffusion coefficient D_B:

$$\Omega = q^2 D_B = 4k_0^2 D_B \sin^2(\theta/2), \tag{3}$$

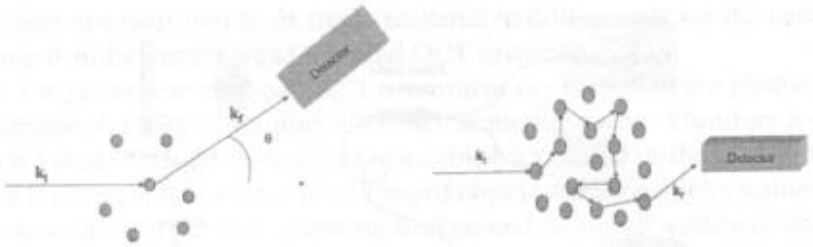

Figure 3. (a) Light propagation through a dilute scattering medium. (b) Light propagation through a dense turbid medium.

where $D_B = k_B T/(3\pi\eta d)$, k_B is the Boltzman constant, T is the temperature of the sample, η is the viscosity of the suspending liquid (in our case H_2O η = 1.0 cps), and d is the hydrodynamic diameter of the scattering particle. Here q denotes the photon momentum transfer, $q = 2k_o \sin(\theta/2)$, where k is the wave number in the scattering medium and θ is the scattering angle. Note that eq. (2) is valid for optical heterodyne detection, while in the case of a homodyne measurement, the expression is multiplied by a factor of two.

In an optically dense medium (Fig. 3b), where light scatters multiple times before detection, the scattering angle, the polarization of the scattered wave and consequently the photon momentum transfer, q, changes with each scattering event. In the case of light diffusion through a turbid medium undergoing Brownian motion, the power spectrum of the detected diffuse light is also a Lorentzian, but with a linewidth dependent on the scattering properties of the suspension and the photon path length within it:

$$\Omega = 2k_0^2 D_B \mu_s (1-g)s\,. \tag{4}$$

Here s is the total path length traveled by the light in the medium, μ_s is the scattering coefficient and g is the scattering anisotropy of the turbid medium defined as an average of the cosine of the scattering angle. For polystyrene microspheres the scattering anisotropy factor and the scattering coefficient can be calculated using Mie theory and the Percus-Yevick structure factors for hard-spheres [21].

For our studies a spectrum analyzer (Stanford Research, SR760) was used to measure the power spectrum of light back scattered from concentrated turbid samples (see Fig. 2). The linewidth and the amplitude of the spectrum were determined by fitting the raw data with a Lorentzian function. The turbid samples used in all experiments were prepared by suspending polystyrene microspheres (Bangs Labs, Inc.) in distilled water. The particle volume fraction in

each monodisperse suspens
length (l_s) of approximatel
temperature, which was re
ments investigating the effe
normalized spatial filter par
diameter was varied betwe

1.2. EXPERIMENTA COHERENCE M

A slightly modified vers
ments (Fig. 2) was used to
standard image resolution
ing medium with known o
on an XYZ translation stag
the layer of scattering med
the cuvette. The imaging
also mounted on an XYZ
point in the medium. The
scanning the focal point ov
measuring the back-scatter
OCM axial and lateral reso
polystyrene microspheres
ticle concentration was cho
of approximately 200 μm.
the objective NA and the c

1.3. MONTE CARL

For our studies we have
detection in OCM geometr
The general principles of
by Jacques and Wang [24].
simulations is presented in
sample surface is used to n
ton direction of propagatio
volume centered at the ch
in the turbid medium acco
[23]. Since we were particu
code was modified to simul
photons by their path lengt

To explore the changes
object within the medium p

ring medium. (b) Light propagation

constant, T is the temperature
g liquid (in our case H_2O η =
f the scattering particle. Here
$2k_o \sin(\theta/2)$, where k is the
he scattering angle. Note that
hile in the case of a homodyne
actor of two.
e light scatters multiple times
ization of the scattered wave
q, changes with each scatter-
a turbid medium undergoing
etected diffuse light is also a
e scattering properties of the

s . (4)

ght in the medium, μ_s is the
otropy of the turbid medium
ering angle. For polystyrene
the scattering coefficient can
ick structure factors for hard-

Research, SR760) was used
ttered from concentrated tur-
e amplitude of the spectrum
rentzian function. The turbid
y suspending polystyrene mi-
he particle volume fraction in

each monodisperse suspension was chosen to result in a photon mean scattering length (l_s) of approximately 100 μm. Samples were kept at a constant room temperature, which was recorded prior to each experiment. For the measurements investigating the effect of the NA on the power spectrum broadening, the normalized spatial filter parameter ν_p ($\nu_p = 2\pi r_p NA/\lambda$), where r_p is the filter diameter was varied between 2 and 6.

1.2. EXPERIMENTAL MEASUREMENTS OF THE OPTICAL COHERENCE MICROSCOPE POINT SPREAD FUNCTION

A slightly modified version of the set-up employed in the Doppler experiments (Fig. 2) was used to measure the OCM axial and lateral resolution. A standard image resolution chart was fixed at a particular position in a scattering medium with known optical properties. The turbid sample was mounted on an XYZ translation stage, which made it possible to alter the thickness of the layer of scattering medium separating the chart from the front surface of the cuvette. The imaging optics in the sample arm of the interferometer was also mounted on an XYZ stage to allow for translation of the objective focal point in the medium. The OCM axial and lateral resolution was evaluated by scanning the focal point over the resolution chart in the X and Z directions and measuring the back-scattered light intensity. The turbid samples used for the OCM axial and lateral resolution measurements were prepared by suspending polystyrene microspheres ($d = 0.22$ μm, $g = 0.2$) in distilled water. The particle concentration was chosen to result in a photon mean scattering length (l_s) of approximately 200 μm. In this particular measurement, the combination of the objective NA and the confocal spatial filter resulted in $\nu_p = 6$.

1.3. MONTE CARLO SIMULATIONS

For our studies we have developed a Monte Carlo code to simulate light detection in OCM geometry for turbid samples with known optical properties. The general principles of our Monte Carlo code are similar to that described by Jacques and Wang [24]. A schematic of the imaging geometry used in all simulations is presented in Fig. 4. A non-uniform photon distribution at the sample surface is used to map out a focused Gaussian beam. The initial photon direction of propagation is determined by simulating a diffraction-limited volume centered at the chosen focal point position. Photons are propagated in the turbid medium according to the rules described by Jacques and Wang [23]. Since we were particularly interested in coherence detection, (OCM), the code was modified to simulate spatial filtering (CM) [24] and gate the detected photons by their path length (OCM).

To explore the changes in the OCM PSF due to a presence of a reflecting object within the medium positioned at the focus of the imaging lens, we have

simulated measurements of the axial and lateral OCM resolution. This was done by moving a perfectly reflecting mirror along the optical axis and transverse to the axis at the beam waist. The Monte Carlo code designed to simulate OCM resolution measurements was used to investigate the dependence of the resolution loss on the objective NA and the sample scattering anisotropy g. Simulations were run for g=0.1, 0.9 and NA=0.1, 0.5. Diffraction theory was used to calculate the confocal lateral and axial resolution in air for the two simulated objectives. For a wavelength of 850 nm and NA=0.1 ($\Delta x = 5\,\mu$m, $\Delta z = 128\,\mu$m), and for NA=0.5 ($\Delta x = 1\,\mu$m, $\Delta z = 5\,\mu$m). The coherence gate parameter corresponding to the SLD coherence length was fixed to $L_c = 10\,\mu$m, which ultimately determined the measurement axial resolution for the small NA lens case. For all simulations the normalized pinhole parameter was fixed to $\nu_p = 7.4$ and the photon scattering length was kept constant ($l_s = 100\,\mu$m). The axial resolution was defined as the FWHM for the normalized intensity profile derived from the simulations, while the lateral resolution was determined as HWHM, where the half maximum (HW) in this case was defined as the middle point between 10% and 90% of the total intensity.

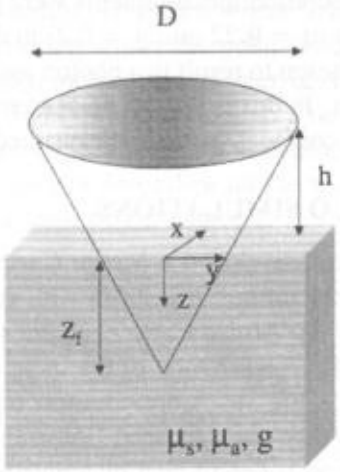

Figure 4. Schematic representation of the Monte Carlo model. D is the diameter of the objective, h is the distance of the objective from the surface of the medium, z_f is the depth of the focal point in the medium.

2. EXPERIMENT RESULTS

The following section re measurements and Monte C in subsections depending or

2.1. DYNAMIC LOW

To demonstrate that DL motion within highly scatte very dilute media, we meas monodisperse suspensions (at a sample depth of 200 μ lengths within the highly sca to avoid Fresnel reflections detection of only single scat Lorentzian (eq. (2)) as indica linewidths obtained from th Brownian diffusion coefficie a backscattered angle of 180° and 0.997 μm) were within 1 spondingly. Multiple experi showed the same accuracy.

To explore the effect of n linewidth we measured the highly scattering, monodisp spheres in water ($g = 0.2$) wi the power spectra measured and 1089 μm below the surf pathlengths of 0.066 mm and lines through the data points normalized to facilitate their longer pathlengths, where th for the 1/f electronic noise th done by directly measuring t fit.

The ability of DLCI to sepa demonstrated with the results transition from single scatter goal the power spectrum wa and all data was fit with a Lo fitting are plotted as a functio

CM resolution. This was done
he optical axis and transverse
rlo code designed to simulate
estigate the dependence of the
mple scattering anisotropy g.
1, 0.5. Diffraction theory was
l resolution in air for the two
m and NA=0.1 ($\Delta x = 5\,\mu$m,
$= 5\,\mu$m). The coherence gate
ngth was fixed to $L_c = 10\,\mu$m,
ial resolution for the small NA
inhole parameter was fixed to
t constant ($l_s = 100\,\mu$m). The
e normalized intensity profile
resolution was determined as
case was defined as the middle
y.

model. D is the diameter of the
e of the medium, z_f is the depth of

2. EXPERIMENTAL AND COMPUTATIONAL RESULTS

The following section reviews all results obtained from the experimental measurements and Monte Carlo simulations. The data presented are organized in subsections depending on the method used.

2.1. DYNAMIC LOW COHERENCE INTERFEROMETRY

To demonstrate that DLCI can be used to image and quantify Brownian motion within highly scattering media in a way similar to DLS methods in very dilute media, we measured the power density spectrum for two separate monodisperse suspensions ($d = 0.22\,\mu$m, $g = 0.2$ and $d = 1.02\,\mu$m, $g = 0.9$) at a sample depth of 200 μm (see Fig. 5), i.e. at a depth of two scattering lengths within the highly scattering medium. This particular depth was chosen to avoid Fresnel reflections from the glass/suspension interface and to ensure detection of only single scattered light. The experimental data was fit with a Lorentzian (eq. (2)) as indicated by the solid lines through the data points. The linewidths obtained from these fits were used to determine the experimental Brownian diffusion coefficients and the corresponding particle sizes, assuming a backscattered angle of 180°. The calculated microsphere diameters (0.222 μm and 0.997 μm) were within 1-5% of the values cited by the manufacturer correspondingly. Multiple experiments with different size polystyrene microspheres showed the same accuracy.

To explore the effect of multiply scattered light detection on the spectrum linewidth we measured the power spectrum as a function of pathlength in a highly scattering, monodisperse suspension of 0.22 μm polystyrene microspheres in water (g = 0.2) with an objective with an NA = 0.2. Figure 6 shows the power spectra measured with the focal point positioned at 33 μm, 792 μm and 1089 μm below the surface of the sample, corresponding to photon total pathlengths of 0.066 mm and 1.584 mm and 2.178 mm respectively. The solid lines through the data points represent the Lorentzian fits. The spectra were normalized to facilitate their comparison. Note that for the measurements at longer pathlengths, where the signal was weaker, it was necessary to account for the 1/f electronic noise that was significant at lower frequencies. This was done by directly measuring the 1/f spectrum and including it in the Lorentzian fit.

The ability of DLCI to separate single scattered from multiply scattered light demonstrated with the results shown in Fig. 7a was further used to explore the transition from single scattered to diffuse light detection. To accomplish this goal the power spectrum was measured in steps of 33 μm inside the sample and all data was fit with a Lorentzian function. The results from the linewidth fitting are plotted as a function of the photon path length in the turbid medium.

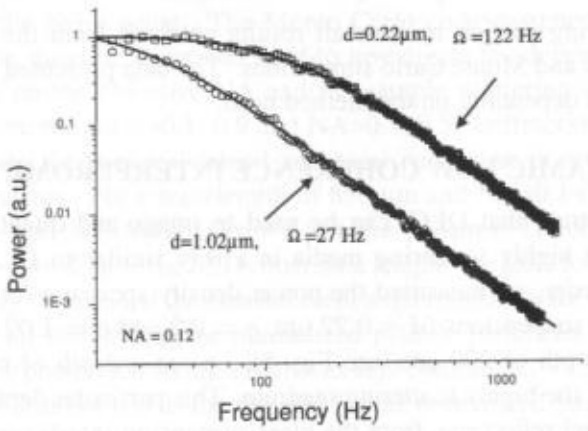

Figure 5. Back-scattered light power spectra measured with DLCI at a depth of 200 μm for two different particle size suspensions. The solid lines through the data points represent the expected Lorentzian profiles. d is the diameter of polystyrene microsphere and Ω is the linewidth of the power spectrum.

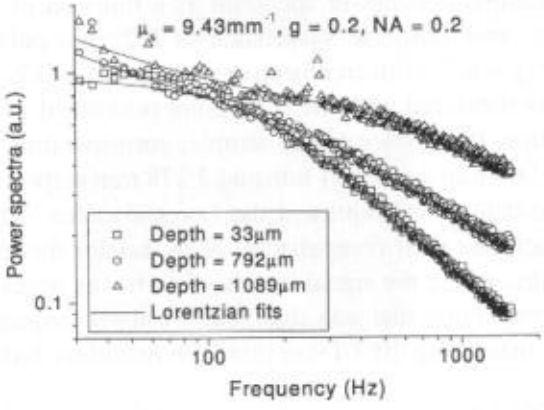

Figure 6. Power spectra measured with DLCI at three different depths inside a highly scattering suspension of microspheres. The solid lines through the data points represent the Lorentzian fits.

The straight lines through t
predicted for the single sc
The arrows on Fig. 7a mar
single scattering, multiply s
arrows was defined the follo
in the spectrum linewidth g
light detection) demonstrate
The corresponding number
to cause such a broadenin
single scattering regime. In
beginning of the light diffu

Figure 7b illustrates the
on the Lorentzian amplitud
practically non-absorbing s
decayed exponentially with
to the scattering coefficien
through the data points repr
theory. The arrows in Fig. 7
regime where light is scatt
graph. The position of th
of the total momentum tra
single scattered, multiply
measurement.

To examine the depende
tropy factor g, power spect
0.39 and 0.75, while keepi
A summary of the experim
is a plot of the data as a fu
($l^* = l_s/(1-g)$) in the me
s/l^* scaling predicted by D
by the linewidth in the sing

To explore the transitio
spectra were measured in a
using three different micro
perimental results are show
is plotted as a function of t
free paths in the medium.
the NA causes the transitio
paths (MFP). Same measu
anisotropy g=0.75 and a su

with DLCI at a depth of 200 μm for two
the data points represent the expected
osphere and Ω is the linewidth of the

z)

ferent depths inside a highly scattering
data points represent the Lorentzian

The straight lines through the data points represent the linewidth behavior as predicted for the single scattering (eq. (2)) and diffusion (eq. (3)) regimes. The arrows on Fig. 7a mark the possible position of the boundaries between single scattering, multiply scattering, and diffusion regimes. The position of the arrows was defined the following way: an assumption was made that a change in the spectrum linewidth greater than 10% of the initial value (single scattered light detection) demonstrates a significant detection of multiply scattered light. The corresponding number of photon mean free paths in the medium, necessary to cause such a broadening of the linewidth was defined as the end of the single scattering regime. In a similar way a limit was established to define the beginning of the light diffusion regime.

Figure 7b illustrates the effect of the detection of multiply scattered light on the Lorentzian amplitude as determined from the fits. As expected, in our practically non-absorbing sample, in the single scattering regime the amplitude decayed exponentially with the path length with an extinction coefficient equal to the scattering coefficient μ_s of the medium ($\mu_s = 1/l_s$). The solid line through the data points represents the decay predicted from the single scattering theory. The arrows in Fig. 7 indicate the beginning and the end of the transition regime where light is scattered a few times as determined from the linewidth graph. The position of the arrows demonstrates clearly that a measurement of the total momentum transfer changes is a better method for separation of single scattered, multiply scattered and diffuse light than a regular intensity measurement.

To examine the dependence of the transition on the sample scattering anisotropy factor g, power spectra were measured in turbid suspensions with g=0.2, 0.39 and 0.75, while keeping the NA of the focusing optics fixed (NA=0.32). A summary of the experimental results is presented in Fig. 8. Note that Fig. 8 is a plot of the data as a function of the number of photon random walk steps ($l^* = l_s/(1-g)$) in the medium rather than scattering lengths (l_s) to utilize the s/l^* scaling predicted by DWS (eq. (3)). Furthermore, the data was normalized by the linewidth in the single scattering regime to facilitate the comparison.

To explore the transition dependence on the imaging lens NA, the power spectra were measured in a suspension with scattering anisotropy factor g=0.2 using three different microscope objectives (NA=0.12, 0.32 and 0.55). The experimental results are shown in Fig. 9a, where the measured spectrum linewidth is plotted as a function of the photon pathlength scaled in terms of photon mean free paths in the medium. The results clearly demonstrate that an increase in the NA causes the transition to occur after a fewer number of photon mean free paths (MFP). Same measurements were repeated for samples with scattering anisotropy g=0.75 and a summary of the results is presented in Fig. 9b.

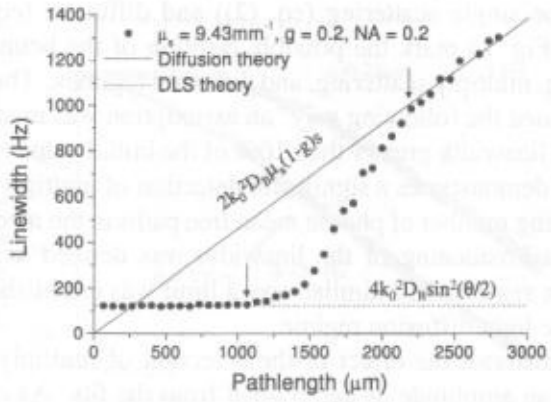

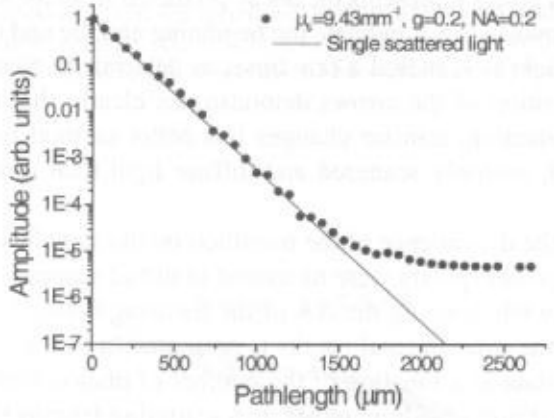

Figure 7. (a) Lorentzian linewidth as a function of photon pathlength in a turbid medium. The dotted and the solid lines indicate the expected linewidth behavior in the single scattering and light diffusion regimes respectively. The arrows indicate the region of photon pathlengths corresponding to detection of multiply scattered but not yet diffuse light. (b) Lorentzian amplitude as a function of photon pathlength in the scattering medium. The solid line represents the expected extinction of single scattered light. The arrows indicate the region of photon pathlengths corresponding to detection of multiply scattered but not yet diffuse light.

2.2. EXPERIMENTAL MEASUREMENTS OF THE OPTICAL COHERENCE MICROSCOPE AXIAL AND LATERAL RESOLUTION

Lateral scans obtained inside the turbid medium demonstrate a clear loss of resolution as the objective focal point is translated deeper into the sample. A

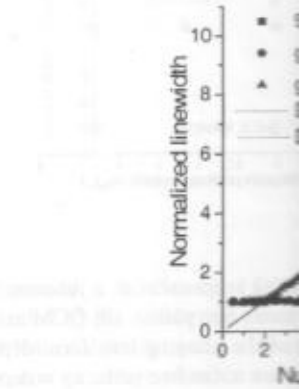

Figure 8. Normalized Lorentz
walks measured in media with th
the solid lines through the data
scattering and light diffusion regi

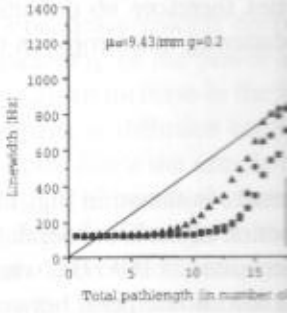

Figure 9. (a) Linewidth as a
a suspension with low scattering
imaging lens. (b) Linewidth as
a suspension with high scattering
imaging lens.

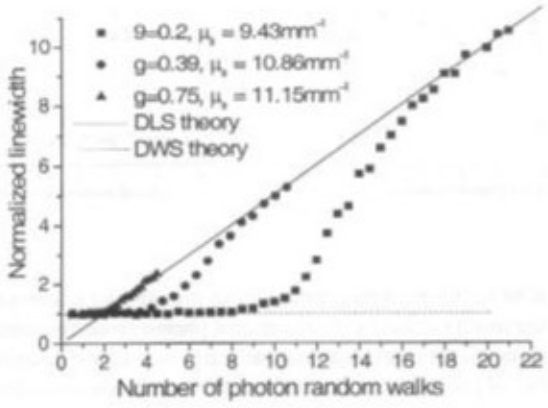

Figure 8. Normalized Lorentzian linewidth as a function of the number of photon random walks measured in media with three different scattering anisotropy factors (g). The dotted and the solid lines through the data points indicate the expected linewidth behavior in the single scattering and light diffusion regimes respectively.

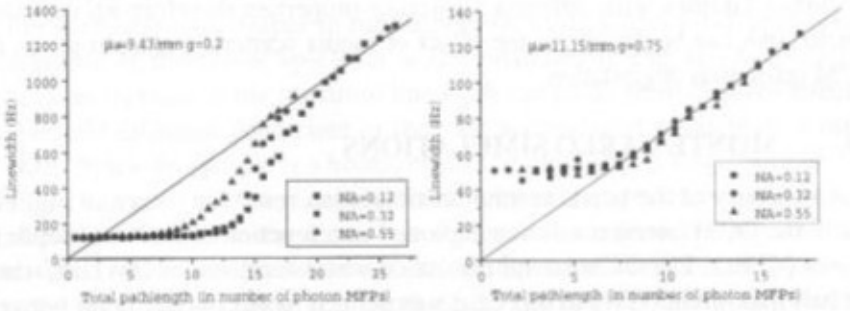

Figure 9. (a) Linewidth as a function of the number of photon mean free paths ($\mu_s s$) in a suspension with low scattering anisotropy (g=0.2) measured for three different NA's of the imaging lens. (b) Linewidth as a function of the number of photon mean free paths ($\mu_s s$) in a suspension with high scattering anisotropy (g=0.75) measured for three different NA's of the imaging lens.

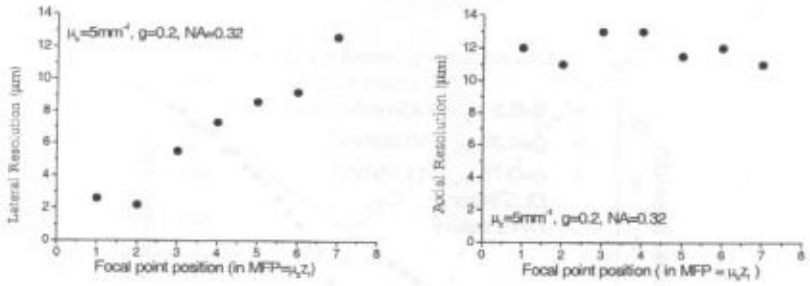

Figure 10. (a) OCM lateral resolution measured in a scattering suspension as a function of the imaging lens focal depth (scaled by the number of photon mean free paths). (b) OCM axial resolution measured in a scattering suspension as a function of the imaging lens focal depth (scaled by the number of photon mean free paths). MFP = photon mean free path. z_f = depth of the focal point.

summary of the experimental results is presented in Fig. 10a where the measured lateral resolution is plotted as a function of the imaging lens focal depth in the scattering suspension in terms of photon MFPs.

A summary of the OCM axial resolution experimental results is presented in Fig. 10b where the measured axial resolution is plotted as a function of the focal point depth. Scans obtained at various depths within the turbid sample demonstrate no apparent change in the OCM axial resolution.

Due to measurement difficulties, no experimental data is currently available for turbid samples with different scattering properties therefore no definitive conclusions can be drawn for the effect of media scattering anisotropy on the OCM resolution degradation.

2.3. MONTE CARLO SIMULATIONS

A summary of the lateral resolution simulation results is shown in Fig. 11a, where the OCM lateral resolution is plotted as a function of the focal depth (in photon MFPs). The OCM lateral resolution was determined as HWHM, where the half maximum (HW) in this case was defined as the middle point between 10% and 90% of the total intensity. The graph presents data for two cases of low and high imaging lens NA and two different suspensions with scattering anisotropy g=0.1 and 0.9.

Simulation results for the axial OCM resolution are summarized in Fig. 11b. The OCM axial resolution was defined as the FWHM for the normalized intensity profile derived from the simulations. The graph represents the axial resolution as a function of the focal depth for four possible combinations of objective lens NA and sample scattering anisotropy.

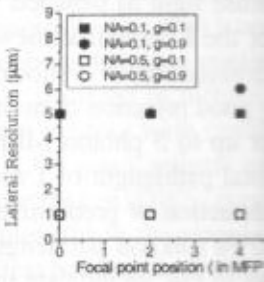

Figure 11. (a) Simulated OCM
(scaled by the number of photo
OCM axial resolution as a funct
photon mean free paths) in a scat

3. DISCUSSION

Initial measurements wit
scattering suspensions reve
DLS theory (Fig. 5). This
is able to reject out of fo
determination of the size of
as a non-invasive, accurate,
sizing in optically dense m

For measurements deep
broadening of the power s
eq. (2), an increase in the s
the particle diffusion coeffi
or both. Since the sample i
constant temperature, the o
attributed to changes in the
from detection of multiply s
that the spectrum acquired
only single scattered light.
1089 μm is in good agreeme
indicating that at such dep
diffuse. The linewidth of th
agree with either the single
the conclusion that in this
completely diffuse. The dat
to distinguish between sing

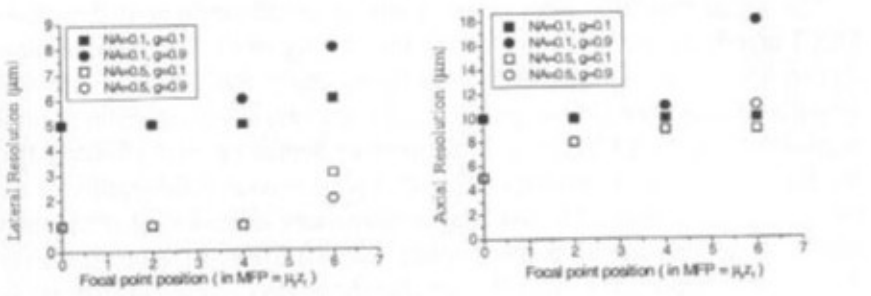

Figure 11. (a) Simulated OCM lateral resolution as a function of the imaging lens focal depth (scaled by the number of photon mean free paths) in a scattering suspension. (b) Simulated OCM axial resolution as a function of the imaging lens focal depth (scaled by the number of photon mean free paths) in a scattering suspension.

3. DISCUSSION

Initial measurements with DLCI at shallow depths (2 photon MFPs) in highly scattering suspensions reveal good agreement between experimental data and DLS theory (Fig. 5). This result demonstrates that at superficial depths DLCI is able to reject out of focus multiply scattered light and to assure precise determination of the size of the scattering particles. Hence DLCI can be applied as a non-invasive, accurate, flexible and inexpensive tool for real-time particle sizing in optically dense media.

For measurements deeper in the suspension though, there is a pronounced broadening of the power spectrum as demonstrated in Fig. 6. According to eq. (2), an increase in the spectrum linewidth can result from changes either in the particle diffusion coefficient or the total accumulated momentum transfer or both. Since the sample is a homogeneous, monodisperse suspension held at constant temperature, the observed broadening of the spectrum could only be attributed to changes in the accumulated photon momentum transfer resulting from detection of multiply scattered light. Comparison with DLS theory reveals that the spectrum acquired at a depth of 33 μm corresponds to detection of only single scattered light. The broadened spectrum measured at a depth of 1089 μm is in good agreement with that predicted by eq. (3) (DWS theory), thus indicating that at such depth the light collected with the DLCI is completely diffuse. The linewidth of the spectrum acquired at a depth of 792 μm does not agree with either the single scattering or light diffusion theories, which leads to the conclusion that in this case the detected light is multiply scattered but not completely diffuse. The data in Fig. 6 clearly demonstrates the ability of DLCI to distinguish between single scattered, multiply scattered and diffuse light.

The actual transition from single scattered to diffuse light as detected with DLCI manifests itself as a non-linear broadening of the Lorentzian linewidth shown in Fig. 7a. As indicated in the figure, the combination of confocal filtering and coherence photon gating results in a very good rejection of multiply scattered background light for measurement depths up to 5 photon MFPs in the turbid suspension (corresponding to a photon total pathlength of 1 mm in the figure). The linewidth data also demonstrates detection of predominantly diffuse light for imaging depths greater than 10 MFPs (photon pathlength of 2 mm). It is important to note though that the arrows in Fig. 7a indicate imaging depths at which multiply scattered and diffuse light become the dominant components of the detected light. The linewidth data exhibits between 2% and 10% deviation from the theoretically calculated value for imaging depths of 2 - 5 photon MFPs in the suspension. Considering that measurement error due to uncertainties in the particle size and concentration and small fluctuations in the sample temperature can amount up to 2%, the spectrum broadening observed for depths greater than 2 and smaller than 5 photon MFPs can be attributed to partial detection of multiply scattered light.

The transition from single scattered to diffuse light as detected with DLCI is also observed as a deviation in the Lorentzian amplitude data from the expected decay in the single scattering regime (Beer-Lambert law) (Fig. 7b). This deviation appears to occur for imaging depths greater than 7 photon MFPs in the scattering medium, though as observed from the linewidth data, at such depths a large portion of the total detected light is multiply scattered. To determine the significance of multiply scattered light detection at shallow imaging depths (2-7 photon MFPs) it is necessary to investigate its effect on the instrument PSF, which is related to image contrast and resolution. Comparison between the data presented in Fig. 7a and Fig. 7b demonstrates that an amplitude measurement lacks the sensitivity for early detection of multiply scattered light and the ability for discrimination between light that has scattered multiple times and light that is completely diffuse. The data in Fig. 7b also raises another question: what source of contrast should an object buried in homogeneous scattering media provide so that the light back-scattered from it raises above the diffuse light background? As determined from the graph, at an imaging depth of 10 photon MFPs (2 mm pathlength) the difference between single scattered and diffuse light intensity is more than two orders of magnitude and the signal light reflected from an object should at least match this difference in order to provide for a minimum image contrast.

Additional experiments performed with different NA's of the imaging objective in turbid samples with a variety of scattering anisotropy factors reveal that the transition from single scattered to diffuse light as detected with DLCI is dependent on the imaging geometry and sample scattering anisotropy. The experimental data shown in Fig. 8 demonstrates that the transition is dependent

on the suspension scattering
isotropically (small g) it occ
In contrast, in turbid media
single scattered to diffuse l
photon random walk (total
Fig. 8. A quick referral to
diffuse regime (DWS) is equ
(pathlength) in the sample i
shortest pathlength at which
measurement the photons m
ing diffuse due to the impos
in mind, the linewidth behav
In the case of highly anisotr
smaller than the NA of the
back-scattered light. In addi
coherence gate causes reject
the snake-like propagation
resulting in small changes o
sition to the diffusion regim
depth of 1 random walk leng
media though, the presence
a significant rejection of mu
the transition to occur at gre

To test how sensitive the
changes in the objective NA
measurements were perform
in Fig. 9a demonstrates that
in a shift of the transition b
photon MFPs (total pathlen
better rejection of multiply
media with low scattering a
in scattering media though,
small NA objectives also res
noise ratio. As expected, si
scattering anisotropy show
NA (Fig. 9b). This result is
biological tissue considerin

The results obtained from
in Fig. 12. The solid lines
for single scattered light de
analytically by Izatt et al.
was used to make adjustm

on the suspension scattering anisotropy, and for samples that scatter light almost isotropically (small g) it occurs after a greater number of photon random walks. In contrast, in turbid media with high scattering anisotropy, the transition from single scattered to diffuse light is very sharp and is centered at a depth of 1 photon random walk (total photon pathlength of 2 random walks as shown in Fig. 8. A quick referral to eq. (2) and eq. (3) shows that the linewidth in the diffuse regime (DWS) is equal to the single scattering linewidth when the depth (pathlength) in the sample is equal to 1 (2) random walk lengths. This is the shortest pathlength at which light can become diffuse. For the geometry of our measurement the photons may have to travel a greater pathlength before becoming diffuse due to the imposed confocal filter and coherence gate. Keeping this in mind, the linewidth behavior as shown in Fig. 8 can be explained as follows. In the case of highly anisotropic media, the lateral spread of the light beam is smaller than the NA of the imaging objective thus ensuring collection of all back-scattered light. In addition, the presence of a confocal spatial filter and a coherence gate causes rejection of only a small portion of the light considering the snake-like propagation of scattered photons close to the lens optical axis resulting in small changes of the photon total pathlength. Therefore, the transition to the diffusion regime in highly anisotropic media occurs at an imaging depth of 1 random walk length. In the case of an almost isotropically scattering media though, the presence of confocal filtering and coherence gating causes a significant rejection of multiply scattered, background light, and thus forces the transition to occur at greater imaging depths.

To test how sensitive the transition from single scattered to diffuse light is to changes in the objective NA for imaging in media with low scattering anisotropy, measurements were performed with NA=0.12, 032 and 0.55 (Fig. 9a). The data in Fig. 9a demonstrates that a five-fold increase in the imaging lens NA results in a shift of the transition boundary positions toward the sample surface by 5 photon MFPs (total pathlength). It is apparent that smaller NA lenses provide better rejection of multiply scattered background light for measurements in media with low scattering anisotropy. If this result is to be applied for imaging in scattering media though, it is necessary to consider the fact that the use of small NA objectives also results in poor spatial resolution and a poor signal-to-noise ratio. As expected, similar measurements performed in media with high scattering anisotropy show no apparent dependence of the transition on the lens NA (Fig. 9b). This result is of particular importance to microscopic imaging of biological tissue considering its high scattering anisotropy.

The results obtained from the DLCI linewidth measurements are summarized in Fig. 12. The solid lines in the graph represent the depth penetration limits for single scattered light detection in CM and OCM in turbid media as derived analytically by Izatt et al. [12]. The analytical model proposed in ref. [12] was used to make adjustments in the position of the solid lines in order to

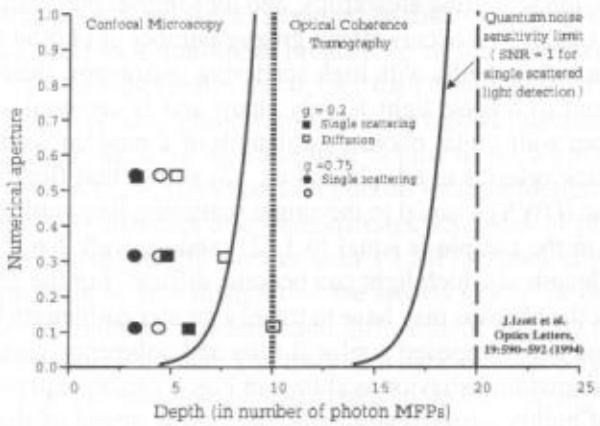

Figure 12. Parametric plot of the theoretical limits of CM and OCM as functions of the focal point depth, scaled by the number of photon mean free paths in the sample. The plot assumes D=7 mm, n_0=1.33, L_c=20 mm, l=850 nm, μ_b=0.3191, μ_s and E=130 mJ (see Izatt[13]). The solid symbols indicate the end of the single scattering regime, while the open symbols correspond to the beginning of the light diffusion regime as determined from the DLCI measurements. The dotted and the dashed lines in the graph indicate the imaging depths at which diffuse light is being detected with DLCI in turbid media with g=0.9 and 0.95 respectively.

suit the imaging parameters of the DLCI system. The data points in Fig. 12 indicate the boundaries between the single scattering, multiply scattering and diffuse regimes as defined from the linewidth data (see arrows in Fig. 7a) for different cases of sample scattering anisotropy and imaging lens NA. (The solid symbols (square and circle) indicate the depths at which multiply scattered light detection causes significant broadening of the spectrum linewidth measured in turbid samples with scattering anisotropy g=0.2 and 0.75. The hollow symbols indicate the experimentally determined imaging depths at which diffuse light becomes the dominant component in the light detected by DLCI. The dotted and the dashed lines in the graph indicate the imaging depths at which DLCI is expected to detect diffuse light in turbid media with g=0.9 and 0.95 respectively.

It is obvious from the graph that though OCM has the dynamic range to provide single scattered light detection in homogeneous turbid media at depths up to 15 photon MFPs, the detected light becomes predominantly diffuse at much shallower imaging depths (except for the case of g=0.95, see dashed line). Better rejection of multiply scattered and diffuse light is observed in cases of almost isotropically scattering media when low NA imaging objectives are used. Another interesting feature observed in the graph is the non-monotonic dependence of the position of the multiply scattered and diffuse light boundaries on the media scattering anisotropy. Due to the confocal and coherence gate rejection of

background light utilized in
g=0.2 appears at depths of 6
the suspension increases to
(toward the sample surface
DWS theory. Further increa
shift of the boundary positio
lines) since highly forward s
before randomization of the
occurs. As mentioned above
can be explained with the fa
ton gating techniques that ve
light in turbid media with lo

Figure 12 reminds us of a
effect of multiply scattered
tion (image contrast and res
and lateral resolution was m
cult cases, a Monte Carlo m
results from the OCM later
demonstrate a clear loss of
ton MFPs. Comparison wi
almost two-fold loss of OCM
cent change in the spectrum
that the presented lateral res
and therefore the chances fo
clusion whether the OCM l
detection of multiply scatter
artifact cannot be reached un
lution data (Fig. 10b) demon
imaging depths that was inve
for the lens used (NA=0.32)
this case is defined by the v
agrees well with the experim
for the range of imaging dep
small linewidth broadening
NA (0.32)in samples with t
the conclusion that in this ca
detection of multiply scattere
imental data is currently ava
properties therefore no defi
media scattering anisotropy

Summarized results from
axial resolution measuremen

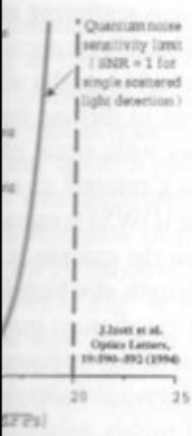

and OCM as functions of the focal
ts in the sample. The plot assumes
and E=130 mJ (see Izatt[13]). The
while the open symbols correspond
from the DLCI measurements. The
ng depths at which diffuse light is
95 respectively.

The data points in Fig. 12
ring, multiply scattering and
a (see arrows in Fig. 7a) for
imaging lens NA. (The solid
hich multiply scattered light
ctrum linewidth measured in
d 0.75. The hollow symbols
epths at which diffuse light
ected by DLCI. The dotted
ing depths at which DLCI is
g=0.9 and 0.95 respectively.
as the dynamic range to pro-
us turbid media at depths up
dominantly diffuse at much
=0.95, see dashed line). Bet-
s observed in cases of almost
ng objectives are used. An-
non-monotonic dependence
light boundaries on the me-
coherence gate rejection of

background light utilized in DLCI, the diffuse light boundary for media with g=0.2 appears at depths of 6-10 photon MFPs. As the scattering anisotropy of the suspension increases to g=0.75, the boundary moves to shallower depths (toward the sample surface) and appears at the position calculated from the DWS theory. Further increase in the scattering anisotropy factor results in a shift of the boundary position deeper into the turbid sample (dotted and dashed lines) since highly forward scattered light requires many more scattering events before randomization of the photon direction of propagation and polarization occurs. As mentioned above, the g dependence of the diffuse boundary position can be explained with the fact that DLCI utilizes confocal and coherence photon gating techniques that very effectively reject multiply scattered background light in turbid media with low scattering anisotropy.

Figure 12 reminds us of a question addressed above: how significant is the effect of multiply scattered background light on the OCM point-spread function (image contrast and resolution). To answer this question, the OCM axial and lateral resolution was measured in turbid media. For experimentally difficult cases, a Monte Carlo model was used to simulate the measurements. The results from the OCM lateral resolution measurement presented in Fig. 10a demonstrate a clear loss of resolution for imaging depths greater than 3 photon MFPs. Comparison with DLCI linewidth data (Fig. 9a) reveals that an almost two-fold loss of OCM lateral resolution corresponds to only a few percent change in the spectrum linewidth at the same imaging depth. Considering that the presented lateral resolution data is derived from a single measurement and therefore the chances for an experimental error cannot be dismissed, a conclusion whether the OCM lateral resolution measurement is very sensitive to detection of multiply scattered background light or the data is a measurement artifact cannot be reached unless measurements are repeated. OCM axial resolution data (Fig. 10b) demonstrates no significant deterioration for the range of imaging depths that was investigated. Considering that the confocal parameter for the lens used (NA=0.32) was 17 μm in water, the OCM axial resolution in this case is defined by the width of the coherence gate (L_c = 13μm) which agrees well with the experimental data. No loss of axial resolution is observed for the range of imaging depths explored. This result compares well with the small linewidth broadening measured with DLCI for the same imaging lens NA (0.32)in samples with the same scattering anisotropy (g=0.2), leading to the conclusion that in this case the OCM axial resolution is not as sensitive to detection of multiply scattered light as OCM lateral resolution. Since no experimental data is currently available for turbid samples with different scattering properties therefore no definitive conclusions can be drawn for the effect of media scattering anisotropy on the OCM resolution degradation.

Summarized results from the Monte Carlo simulations of OCM lateral and axial resolution measurements in turbid media are presented in Fig. 11a and

Fig. 11b correspondingly. The results in Fig. 11a demonstrate no significant change in the lateral OCM resolution for the case of high NA imaging lens for depths in the scattering medium smaller than 4 photon MFPs (hollow squares and circles). This behavior appears to be independent of the sample scattering anisotropy. For depths greater than 4 MFPs, a rapid degradation of the OCM lateral resolution is observed and it is more pronounced for suspensions with low g factor. For the case of small NA of the imaging objective, simulation results also show deterioration of the OCM lateral resolution, though not as rapid as in the case of high NA (solid squares and circles). The resolution degradation appears to be more pronounced and to occur at shallower depths for media with high scattering anisotropy. This result compares very well with the DLCI experimental data where the effect of the multiply scattered light on the OCM PSF is measured as a total change in spectrum linewidth. Changes in OCM lateral resolution (Fig. 11a) are apparent for photons that had traveled between 6 and 16 mean paths in the scattering suspension (corresponding to focal depths of 3 to 8 photon MFPs) and for the same range of photon paths broadening of the Lorentzian linewidth is also observed (Fig. 9a and Fig. 9b).

Summarized results from the OCM axial resolution simulations are presented in Fig. 11b. As we have seen experimentally, for the case of an almost isotropically scattering background, there is no change in the axial resolution for small NA and depths less than 7 photon MFPs, where the resolution is determined by the coherence length Lc of the light source. A small change in the axial resolution is observed for an NA=0.5 for the same background sample properties for shallow depths where there is a transition from the value predicted for non-scattering media to almost the full width of Lc. In the case of background with high anisotropy factor (g=0.9) there is a pronounced loss of OCM axial resolution with imaging depth for simulations with both small and large NA. Again, loss of axial resolution is observed for a region of photon MFPs in turbid media corresponding to a pronounced spectrum broadening measured with DLCI (Fig. 9a,b). A possible explanation for the observed OCM resolution dependence on sample optical properties and instrument imaging geometry is that in a medium with high scattering anisotropy, light scatters preferentially in the forward direction resulting in a relatively small lateral spread of the light beam. The small-angle scattering also causes a snake-like propagation of the scattered photons, causing small increase of the total photon pathlength compared to the case of photon ballistic travel from the sample surface to the lens focal point position and back. Therefore, the confocal filter and the coherence gate do not provide good rejection of multiply scattered light thus causing rapid and pronounced loss of both axial and lateral OCM resolution at shallower imaging depths. For the case of measurements in almost isotropically scattering media the combination of small NA lens and a coherence gate results in preferential

detection of single scattered
apparent change in the meas

Though the simulation res
lateral resolution in scatterin
ration effect is not as dramati
It is imperative to point out a
measurement was made and
ther investigation is necessa
experimental and the simula

Summary

In summary, a number of
to study the process of mult
on image resolution. A new
total momentum transfer occ
investigate the transition fro
tem applying confocal and
results demonstrated the ab
tered, multiply scattered an
imaging depth (as a functio
NA) at which a dominant po
tion other experimental and
multiply scattered light, ma
(DLCI), causes significant
that the deterioration effect
imaging lens NA. Though
to some of the questions ra
are left unanswered and ev
still unclear what the OCM
g and lens NA) and whethe
noise ratio or the signal-to-
degradation exclusively du
carry any information abou
light reflected off the obje
above also responsible for
will be addressed in our fu

References

[1] J. Powley, *Handbook*
New York, 1995).

[2] R. Webb, Rep. Prog.

detection of single scattered light at shallow imaging depths, thus causing no apparent change in the measured OCM axial and lateral resolution.

Though the simulation result presented in Fig. 11a demonstrate loss of OCM lateral resolution in scattering media as the imaging depth increases, the deterioration effect is not as dramatic as observed in the experimental results (Fig. 10a). It is imperative to point out again that due to the fact that only one experimental measurement was made and due to the high chance for experimental error, further investigation is necessary to reveal whether the discrepancy between the experimental and the simulation data is real.

Summary

In summary, a number of experimental and computational methods were used to study the process of multiply scattered light detection in OCM and its effect on image resolution. A new method (DLCI), sensitive to changes in the photon total momentum transfer occurring in the process of scattering, was employed to investigate the transition from single scattered to diffuse light in an imaging system applying confocal and coherence photon gating techniques. Experimental results demonstrated the ability of DLCI to discriminate between single scattered, multiply scattered and diffuse light and allowed for determination of the imaging depth (as a function of sample scattering anisotropy and imaging lens NA) at which a dominant portion of the detected light becomes diffuse. In addition other experimental and computational results revealed that the detection of multiply scattered light, manifesting itself as a spectrum linewidth broadening (DLCI), causes significant lateral and axial OCM resolution degradation and that the deterioration effect is dependent on the media scattering anisotropy and imaging lens NA. Though the work presented in this chapter provides answers to some of the questions raised in the introduction of this paper, some of them are left unanswered and even accompanied with a few more. For example, it is still unclear what the OCM image penetration depth is (as a function of sample g and lens NA) and whether this depth is limited by the measurement signal-to-noise ratio or the signal-to-background ratio. Furthermore, is image resolution degradation exclusively due to background light detection (light that does not carry any information about the imaged object buried in the turbid media) or is light reflected off the object and multiply scattered traversing the turbid layer above also responsible for loss of image resolution? These questions and more will be addressed in our future studies.

References

[1] J. Powley, *Handbook of biological confocal microscopy* (Plenum Press, New York, 1995).

[2] R. Webb, Rep. Prog. Phys. **59**, 427-471 (1996).

[3] M. Rajadhyaksha, Appl. Opt. **38**, 2105-2115 (1999).

[4] D. Huang, E. A. Swanson, C. P. Lin, J. S. Schuman, W. G. Stinson, W. Chang, M. R. Hee, T. Flotte, K. Gregory, C. A. Puliafito and J. G. Fujimoto, Science **254**, 1178-1181 (1991).

[5] J. Schmitt,A. Knuttel, A. H. Gandjbakhche and R. F. Bonner, Proc. SPIE **1889**, 197-211 (1993).

[6] B. Bouma, Opt.Lett. **20**, 1486-1488 (1995).

[7] A. Yodh and B. Chance, Phys. Today, **48**, 34-40 (1995).

[8] S. Arridge, Inverse Problems, **15**, R41-R94 (1999).

[9] M. Kempe, A. Z. Genack, W. R. Dorn and P. Dorn, J. Opt. Soc. Am. A **14**, 216-223 (1997).

[10] M. Kempe, J. Opt. Soc. Am. A **13**, 46-52 (1996).

[11] M. Yadlowsky, J. M. Schmitt and R. F. Bonner, Appl. Opt. **34**, 5699-5707 (1995).

[12] J. Izatt, M. R. Hee, G. M. Owen, E. A. Swanson and J. G. Fujimoto, Opt. Lett. **19**, 590-592 (1994).

[13] Y. Pan, R. Birngruber and R. Engelhardt, Appl. Opt. **36**, 2979-2983 (1997).

[14] D. A. Boas, K. K. Bizheva and A. M. Siegel, Opt. Lett. **23** (1998).

[15] K. Bizheva, D. A. Boas, Phys. Rev. E, **58**, 7664-7667 (1998).

[16] P.J. Berne and R. Pecora, (Wiley, New York, 1976).

[17] R. Pecora, (Plenum Press, New York, 1985).

[18] D. J. Pine, D. A. Weitz, P. M. Chaikin and E. Herbolzheimer, Phys. Rev. Lett. **60**, 1134-1137 (1988).

[19] G. Maret and P. E. Wolf, Z. Phys. B **65**, 409-413 (1987).

[20] D. Durian, Phys. Rev. E **51**, 3350-3358 (1995).

[21] P. Kaplan, M. H. Kao, A. G. Yodh and D. J. Pine, Appl. Opt. **32**, 3828-3836 (1994).

[22] A. Yodh, P. D. Kaplan and D. J. Pine, Phys. Rev. B **42**, 4744-4747 (1990).

[23] S. L. Wang, S. L. Jacques, and L. Zheng, Computer Methods and Programs in Biomedicine **47**, 131-146 (1995).

[24] A.K. Dunn, C. Smithpeter, A.J. Welch and R. Richards-Kortum, Appl. Opt. **35**, 3441-344 (1996).

Chapter 2

SCATTERING BY
BETWEEN RADI
ELECTROMAGN

J.-J. Greffet and J.B. Thiba
Laboratoire EM2C, U.P.R. 288 C
92295 Châtenay-Malabry Cedex,
greffet@em2c.ecp.fr

L. Roux, P. Mareschal and
Dassault-Aviation
92552 Saint-Cloud Cedex 300, Fr

Abstract The paper is devo
randomly located
has been solved nu
a numerical soluti
as forward scatter
radiative transfer
thick systems wh
have also shown t

Keywords: scattering, radiativ

Introduction

Propagation of waves in
theories. The simplest app
of radiative transfer. The
[1], which describes the pro
properties of the medium a
volume in order to account
realize that the phase of th

P. Sebbah (ed.), Waves and Imaging